Sorption enhanced carbon dioxide hydrogenation to methanol: Process design and optimization

Maksimov Pavel, Nieminen Harri, Laari Arto, Koiranen Tuomas

DOI: 10.1016/j.ces.2022.117498

Chemical Engineering Science 252 (2022) 117498

Contents lists available at ScienceDirect

Chemical Engineering Science

journal homepage: www.elsevier.com/locate/ces

Sorption enhanced carbon dioxide hydrogenation to methanol: Process design and optimization

Pavel Maksimov *, Harri Nieminen, Arto Laari, Tuomas Koiranen

Lappeenranta-Lahti University of Technology, LUT School of Engineering Science, Yliopistonkatu 34, 53850, P.O. Box 20, FI-53851 Lappeenranta, Finland

HIGHLIGHTS

- Sorption enhanced CO_2 hydrogenation to methanol is studied via process modeling.
- Reactor model is based on experimentally validated kinetic data.
- Dynamic model considers unreacted gases recirculation and product separation.
- Process parameters for production of high purity methanol product are determined.

ARTICLE INFO

Article history:
Received 26 October 2021
Received in revised form 27 January 2022
Accepted 3 February 2022
Available online 7 February 2022

Keywords:
Methanol synthesis
Sorption enhanced
CO_2 hydrogenation
Process intensification
Optimization

ABSTRACT

Sorption enhanced synthesis has been previously shown to improve carbon dioxide hydrogenation to methanol by mitigating the thermodynamic limitations. This work investigates the efficiency of methanol synthesis via sorption enhanced carbon dioxide hydrogenation focusing on determining the optimal process parameters. The study is based upon a fully dynamic experimentally validated model of the process which is extended to account for adsorbent regeneration, downstream product separation and recirculation of the unreacted gases. An additional reactor configuration with a guard adsorbent layer is proposed for production of high purity methanol product. A multi-objective optimization study is performed to investigate the tradeoff between methanol production rate and product purity. The obtained results indicate that for synthesis of high purity methanol product, the optimal values of reactor temperature and catalyst mass fraction in the bed are 215 °C/0.65 and 235 °C/0.50 for the adiabatic and quasi-isothermal reactors, respectively.

1. Introduction

Methanol is one of the most important commodity chemicals in the world and global demand for methanol is constantly growing. Not only does methanol serve as a precursor for the synthesis of a wide variety of essential chemicals, it can also be used as a clean-burning transportation fuel or as a hydrogen carrier in fuel cells (Kung, 1994; Gurau et al., 2020). Conventionally, methanol is produced by catalytic conversion of syngas over Cu/ZnO catalysts under pressure of 50–100 bar and temperature of 200–250 °C (Fiedler Eckhard et al., 2007). Methanol synthesis proceeds via the following reactions:

$$CO + 2H_2 \rightleftharpoons CH_3OH \quad \Delta H^0 = -91.0\text{kJ/mol} \tag{1}$$

$$CO_2 + H_2 \rightleftharpoons CO + H_2O \quad \Delta H^0 = 41.2\text{kJ/mol} \tag{2}$$

$$CO_2 + 3H_2 \rightleftharpoons CH_3OH + H_2O \quad \Delta H^0 = -49.8\text{kJ/mol} \tag{3}$$

As indicated by Eq. (3), methanol can also be produced via direct hydrogenation of carbon dioxide. In principle, this process is forecast to play a pivotal role in the decoupling of the chemical industry from fossil-based resources (Kätelhön et al., 2019). However, this route is much less efficient in view of the severe equilibrium limitations originating from the stability of the carbon dioxide molecule (Westerterp et al., 1989). Moreover, without carbon monoxide in the feed, formation of water via the reverse water gas shift reaction (Eq. (2)) increases, further exacerbating the thermodynamic limitations (Arena et al., 2007). An additional issue posed by the excessive formation of water is its detrimental impact on the catalytic material, which is mainly associated with inhibition of catalyst active sites (Ma et al., 2009; Sahibzada et al., 1998).

In-situ removal of water has been recognized as a promising intensification strategy for alleviating the thermodynamic

* Corresponding author.
E-mail address: pavel.maksimov@lut.fi (P. Maksimov).

https://doi.org/10.1016/j.ces.2022.117498
0009-2509/

Nomenclature

Greek symbols

ε_b	bed porosity;
ε_p	particle porosity;
ε_t	total bed porosity (considers the total void volume $\varepsilon_t = \varepsilon_b + (1-\varepsilon_b)\varepsilon_p$);
$\rho_{ads,p}$	adsorbent particle density, kg/m^3;
ρ_{ads}	adsorbent bulk density, kg/m^3;
ρ_{cat}	catalyst bulk density, kg/m^3;
ρ_w	reactor wall density, kg/m^3;
$\vartheta_{i,j}$	stoichiometric coefficient of component i for reaction j;
μ	gas dynamic viscosity, Pa s;
η_j	effectiveness factor of reaction j;
τ_{HP}	flow residence time in the high-pressure flash drum, s;

Other symbols

$b_{H_2O,0}$	Langmuir adsorption isotherm fitting parameter, Pa^{-1};
b_{H_2O}	Langmuir adsorption isotherm parameter, Pa^{-1};
$C_{p,ads}$	adsorbent heat capacity, J/(kg K);
$C_{p,cat}$	catalyst heat capacity, J/(kg K);
$C_{p,g}$	gas heat capacity, J/(mol K);
C_{p,H_2O}	adsorbate heat capacity, J/(mol K);
$C_{p,w}$	reactor wall material heat capacity, J/(kg K);
D_c	micropore diffusivity, m^2/s;
D_l	axial dispersion coefficient, m^2/s;
D_p	macropore diffusivity, m^2/s;
F_f	flowrate of the make-up stream during the reaction step, mol/s;
$F_{gas,HP}$	flowrate of the top product of the high-pressure flash drum, mol/s;
$F_{liq,HP}$	flowrate of the bottom product of the high-pressure flash drum, mol/s;
$F_{liq,LP}$	flowrate of the bottom product of the low-pressure flash drum, mol/s;
F_{out}	flowrate of the reactor outlet stream during the reaction step, mol/s;
F_r	flowrate of the recycle stream during the reaction step, mol/s;
f_i	partial fugacity of component i, bar;
h_{in}	reactor wall - catalyst/adsorbent mixture heat transfer coefficient, J/(m^2 K s);
h_{out}	reactor wall - reactor wall surroundings heat transfer coefficient, J/(m^2 K s);
K_i	adsorption constant of component i, bar^{-1};
$K_{p,j}$	equilibrium constant of reaction j;
k_{LDF}	mass transfer coefficient for water adsorption on the adsorbent, s^{-1};
k_f	film mass-transfer coefficient for water adsorption on the adsorbent, s^{-1};
k_j	kinetic constant of reaction j, mol/(s bar kg$_{cat}$);
k_w	reactor wall axial thermal effective conductivity, J/(kg K s);
k_z	bed axial effective thermal conductivity, J/(kg K s);
L	reactor length, m
m_{H_2O}	adsorbent saturation capacity, mol/kg;
p	reactor pressure, Pa;
p_h	reactor pressure during the reaction step, Pa;
p_l	reactor pressure during the regeneration step, Pa;
q	adsorbent loading, mol/kg;
q^*	equilibrium adsorbent loading, mol/kg;
R	universal gas constant, J/(mol K);
R_j	rate of reaction j per weight of catalyst, mol/(s kg$_{cat}$) ;
r_c	micropore radius, m;
r_{in}	inner reactor radius, m;
r_{out}	outer reactor radius, m;
r_p	average particle radius, m;
T_{out}	reactor wall surroundings temperature, K;
T_{reac}	reaction step temperature, K;
T_w	reactor wall temperature, K;
T	bed temperature, K;
t	time, s;
t_{cycle}	total cycle duration, min;
t_p	time step during reaction step simulation, s;
t_{pres}	pressurization step duration, s;
t_{depr}	depressurization step duration, s;
v	interstitial gas velocity, m/s;
$x_{i,HP}$	component molar fraction in the bottom product of the high-pressure flash drum;
$x_{i,LP}$	component molar fraction in the bottom product of the low-pressure flash drum;
y_i	component molar fraction in the reactor;
$y_{i,HP}$	component molar fraction in the top product of the high-pressure flash drum;
$y_{i,LP}$	component molar fraction in the top product of the low-pressure flash drum;
$y_{i,inlet}$	component molar fraction at the reactor inlet during the reaction step;
y_f	component molar fraction in the make-up stream;
y_r	component molar fraction in the recycle stream;
z	axial coordinate over the reactor length, m;
$\Delta H_{ads,H_2O}$	heat of water adsorption on the adsorbent, J/(mol);
$\Delta H_{R,j}$	heat of reaction j, J/(mol);

List of Acronyms:

SE	Sorption-Enhanced;
DME	Dimethyl ether;
GHSV	Gas Hourly Space Velocity;
PDEs	Partial Differential Equations;
ODEs	Ordinary Differential Equations;
PSA	Pressure Swing Adsorption
VLE	Vapor Liquid Equilibrium;

limitations and thereby facilitating the methanol synthesis reactions (van Kampen et al., 2021). In general, the two main technologies considered most suitable for in-situ water removal are membrane-based separation and adsorption (van Kampen et al., 2019), although other separation methods have also been proposed (van Bennekom et al., 2013; Reichert et al., 2019; Bos and Brilman, 2015). The membrane-based separation strategy involves conducting the synthesis in a membrane reactor, where removal of products is achieved by selective permeation through the membrane. In the case of adsorption, a reactor column is packed with a mixture of catalyst and adsorbent, with the latter serving as a water retaining agent. This technique is generally referred to as sorption enhanced (SE) synthesis (Carvill et al., 1996). Although, SE synthesis provides an opportunity to greatly increase both single-pass conversion and product selectivity, the process requires periodic regeneration of the adsorbent due to its limited sorption capacity. However, when applied to methanol production, SE synthesis technology is preferable over the membrane-based separation route. Elevated process temperatures required for the methanol synthesis reactions (Eqs. 1–3) make application of polymeric membranes impossible because of their unsatisfactory thermal stability properties (Li et al., 2021). While inorganic membranes, such as zeolite

membranes, are more stable under harsh thermal conditions, they typically exhibit lower permselectivities for water molecules under the methanol synthesis conditions due to weak water adsorption at higher temperatures (Sandström et al., 2010; Lee et al., 2018; Zhu et al., 2005). Although very promising results have been reported by Li et al. (Li et al., 2020), who have demonstrated highly efficient carbon dioxide hydrogenation to methanol in a lab-scale membrane reactor, application of membrane reactors for industrial scale methanol production currently remains impractical due to numerous design challenges. Particularly, scaling-up of the preparation of high-quality membranes and making gas-tight membrane modules that can withstand methanol synthesis conditions are some of the major hindrances in terms of industrial-scale implementation of the process (Li et al., 2021).

SE synthesis is widely recognized as an intensification strategy holding much promise particularly in application to thermodynamically limited hydrogeneration reactions. The SE synthesis concept has been utilized to intensify processes such as carbon dioxide methanation (Borgschulte et al., 2013), the water gas shift reaction (Boon et al., 2017; Hu et al., 2019) methanol and dimethyl ether (DME) synthesis (van Kampen et al., 2021; van Kampen et al., 2020; Van Kampen et al., 2021). SE synthesis of methanol is of particular interest in conjunction with downstream product processing since, unlike SE DME synthesis (Skorikova et al., 2020), the process confers an advantage of simplified product separation. Methanol and water, being the only liquid products, are easily separated from the other components involved in the synthesis. Therefore, if water is selectively retained by the adsorbent, a highly concentrated methanol product can be obtained without elaborate downstream purification.

Although experimental investigation of methanol synthesis via SE carbon dioxide hydrogenation remains rather limited so far, it has been demonstrated that in-situ removal of water indeed improves methanol production. However, the increase in production rate was reported to be more significant for carbon monoxide (Terreni et al., 2019). Moreover, in our previous work (Maksimov et al., 2021), the acquired experimental data were shown to deviate considerably from the predictions of the reactor model based on the well-established kinetic interpretation of methanol synthesis (Graaf et al., 1988). In a recent study on the topic of SE methanol synthesis catalysis, Nikolic et al. (Nikolic et al., 2021) reported that varying water partial pressure influences individual steps of the methanol synthesis reactions. More specifically, the study found that under SE methanol synthesis conditions, due to in-situ water adsorption, a considerable amount of reaction intermediates is formed and accumulated before being converted to the end products. These findings correlate with the aforementioned discrepancies between the experimental observations and the reactor simulation results and also indirectly substantiate the updated kinetic constants (Maksimov et al., 2021) proposed for more accurate description of the system.

A plethora of research efforts has been devoted to investigation and optimization of SE methanol synthesis via mathematical modeling of the process. A rigorous thermodynamic analysis of carbon dioxide hydrogenation to methanol with in-situ water sorption has been performed by Zachopoulos and Haracleous (Zachopoulos and Heracleous, 2017). Simulating the steady-state performance of methanol synthesis reactor by minimizing the Gibbs free energy of the input reactants, they have reported a consistently higher methanol yield for the SE carbon dioxide hydrogenation process. Arora et al. have developed a generalized framework for dynamic simulation of SE processes (Arora et al., 2018), and with it, they have analyzed the optimal performance of an SE methanol synthesis reactor (Arora et al., 2018). Bayat et al. have also conducted several studies focusing on dynamic modeling and optimization of SE methanol synthesis and proposing conceptually novel reactor configurations for the process (Bayat et al., 2014; Bayat et al., 2014; Bayat et al., 2016). Although these studies capture the dynamic nature of the SE methanol synthesis process, they are based on the kinetic model that has been developed for steady state methanol synthesis and does not take into account the effect of in-situ removal of water. Furthermore, the modeling of non-reacted gases recirculation is not sufficiently addressed either.

Therefore, to accurately evaluate the process performance, this work is based on an experimentally validated dynamic model of the reactor for SE carbon dioxide hydrogenation to methanol (Maksimov et al., 2021). The model is extended to account for adsorbent regeneration and downstream product separation. Considering that in-situ removal of water significantly enhances carbon monoxide production, a particular emphasis is given to the dynamic simulation of the unreacted gases recirculation.

This work analyzes the performance of a semi-industrial-scale unit for methanol synthesis via SE carbon dioxide hydrogenation focusing on the methanol production rate and product quality. Since the process requires periodic regeneration of the adsorbent, a system of several reactor columns is needed to achieve quasi-continuous operation. The total number of reactors and overall cycle design can be tuned to accommodate a given regeneration procedure. However, the specific methanol production rate and product purity are not affected by the total number of the reactors. Therefore, instead of restricting the study by specifying the total number of the reactors, a system comprising of a single reactor is investigated focusing on maximizing the specific production rate. A series of parametric and optimization studies is conducted to determine optimal operating conditions and analyze the tradeoff between specific methanol production rate and product purity.

2. Methodology

In this work, two different reactor configurations for SE methanol synthesis are investigated. In one reactor configuration, the SE methanol synthesis is carried out in a tubular reactor that is kept at constant temperature over the entire process cycle. The compressed reacting gases flow through the tube side filled with a mixture of catalyst and adsorbent, while on the shell side, boiling water maintains a near constant temperature regime within the reactor. Since, owing to the highly transient nature of the SE methanol synthesis process, some variations in the bed temperature cannot be avoided, this reactor is termed '*quasi-isothermal*'. In the other configuration, the temperature inside a fixed-bed reactor filled with a catalyst-adsorbent mixture is not controlled. Hence, this configuration is labelled '*adiabatic*'. In this case, the in-situ water adsorption and the enhanced exothermic hydrogenation reactions (Eqs. (1) and (3)) considerably increase the bed temperature during the SE methanol synthesis. Therefore, subsequent regeneration step, which involves water desorption from the adsorbent, is significantly improved because of the elevated bed temperature.

For practical comparison, the dimensions of the studied reactors were adjusted so that the total bed volume consisting of catalyst and adsorbent is equal for both reactor configurations. The dimensions of the reactors are provided in Table 1 along with catalyst and adsorbent bulk density values. In view of the scale of the investigated process, the average spherical particle diameter was selected as 4 mm for both catalyst and adsorbent. Feed gas consisted of a stoichiometric (1:3) mixture of carbon dioxide and hydrogen. A 3 Å molecular sieve was selected as a water adsorbent due to its high capacity under elevated temperature conditions and non-interference with the process selectivity (Maksimov et al., 2021; Nieminen et al., 2018), which is an issue with larger pore size adsorbents (Terreni et al., 2019; Nikolic et al., 2021).

Table 1
Reactor and process parameters.

Parameter	Value
Adiabatic reactor diameter, m	2
Adiabatic reactor height, m	8
Adiabatic reactor wall thickness, mm	100
Quasi-isothermal reactor tube diameter, m	0.035
Quasi-isothermal reactor tube length, m	7
Quasi-isothermal reactor tube wall thickness, mm	2
Quasi-isothermal reactor tubes quantity	3750
Average particle diameter, mm	4
Adsorbent bulk density, kg/m^3	600
Catalyst bulk density, kg/m^3	1500
CO_2:H_2 ratio in the feed	1:3

The complete process cycle is assumed to consist of the following steps operated in a consecutive manner: reactor pressurization, SE reaction, reactor depressurization and adsorbent regeneration. The flow of the gases during the depressurization and adsorbent regeneration steps is arranged in the direction opposite to that of the flow of the gases during the reactor pressurization and SE reaction steps. This arrangement enables more efficient desorption of water from the adsorbent (Arora et al., 2018). During the pressurization and depressurization steps, the reactor pressure is considered to change linearly. Although more complex and advanced adsorbent regeneration schemes have been reported, for example a temperature–pressure swing adsorption (van Kampen et al., 2020) or a five-step pressure swing adsorption (Leperi et al., 2019), the selected design confers the advantage of simplicity, and it was thus deemed most suitable for the purpose of the current optimization study. Fig. 1 provides a general overview of the process.

In general, for fixed reactor dimensions, the main process parameters subject to optimization are pressure and temperature conditions, gas hourly space velocity (GHSV), and catalyst-adsorbent mixture composition. Except for the catalyst-adsorbent mixture, these parameters might differ for reaction and regeneration steps of the cycle. Additionally, the duration of the reaction and regeneration steps are also adjustable parameters, which significantly affect the process performance. Considering the dynamic nature and complexity of the studied process, optimization of these parameters is an exceptionally demanding task in terms of computational resources, since simulating even a single reaction-regeneration cycle might be time-consuming because of the small integration step size required to resolve sharp fronts of concentrations and temperature propagating through the reactor. In this regard, since increasing the reactor pressure not only facilitates the hydrogenation reactions (Eqs. (1) and (3)) but also improves water adsorption, the effect of pressure is omitted in this study due to its obvious beneficial impact on the process efficiency. Moreover, to a great extent, selection of the optimal reactor pressure during the reaction step is a matter of economic optimization, which is out of the scope of the current study. Therefore, the reactor pressure during the SE reaction step is fixed at 50 bar. This value is practical for industrial scale methanol synthesis reactor (Nieminen et al., 2019; Nyári et al., 2020), and it was also covered during the experimental investigation of SE carbon dioxide hydrogenation process (Maksimov et al., 2021).

Considering the selected reaction step pressure and taking the data of Boon et al. (Boon et al., 2017; Boon et al., 2015) as a

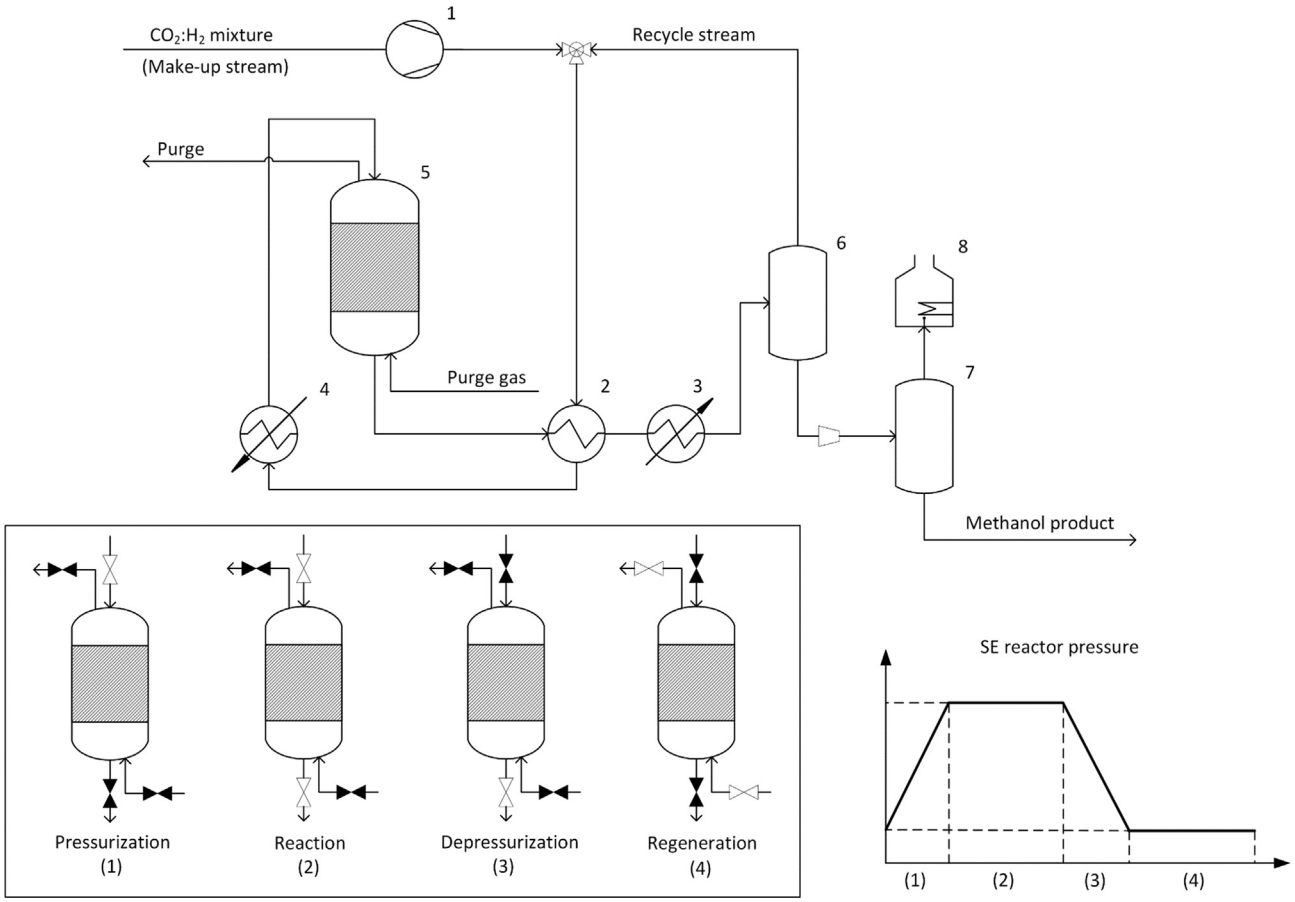

Fig. 1. Flowsheet of the SE methanol synthesis process 1 – compressor; 2 – heat exchanger; 3 – cooler; 4 – heater; 5 – SE reactor; 6 – high pressure flash drum; 7 – low pressure flash drum; 8 – purge gas combustor.

reference, the duration of the pressurization step is set as 5 min to ensure safe and reliable operation of the reactor. The same duration is set for the depressurization step. The GHSV values are set to be equal for reaction and regeneration steps. As heating and cooling of the reactor are time-consuming operations (van Kampen et al., 2020), in the quasi-isothermal configuration, the reactor temperature is set to be equal for reaction and regeneration steps.

2.1. Process description

During the reactor pressurization step, the reactor column is pressurized with a stoichiometric (1:3) mixture of carbon dioxide and hydrogen. The gases are fed to the reactor inlet, while the reactor outlet is sealed. Since the reactor is already heated to the required temperature before the pressurization, the reactions and, hence, water adsorption begin already at this stage. Due to the overall exothermicity of the reactions and water adsorption, this results in a moderate increase of the bed temperature for the adiabatic reactor configuration and minor heat production for the quasi-isothermal reactor configuration.

Once the required reactor pressure is reached, the reaction step is commenced. During this step, both the reactor inlet and outlet are open, and the product stream is cooled and sent to the high-pressure flash separation unit. To facilitate condensation of the obtained methanol product, the flash separation unit is maintained at reactor pressure and ambient temperature. The top product of the flash drum is heated up to the process temperature and recycled back to the reactor. Constant inflow in the reactor is maintained by addition of a fresh stoichiometric (1:3) mixture of carbon dioxide and hydrogen to the recycled stream.

During the course of the SE reaction step, the conversion of the inlet reactants gradually decreases as the adsorbent gets saturated with water. As a result, since complete recirculation of the non-condensables is considered, the flowrate of the recirculated stream increases during the reaction step while the flowrate of the fresh make-up stream decreases. This design provides an opportunity to maximize the conversion of the initial reactants and at the same time allows for efficient use of the carbon monoxide that is produced in large quantities during the sorption enhanced carbon dioxide hydrogenation.

The bottom product of the high-pressure flash separation unit, consisting predominantly of methanol, is further processed to the low-pressure flash separation unit, where trace amounts of dissolved carbon monoxide, carbon dioxide and hydrogen are removed. Due to the exothermicity of the enhanced hydrogenation reactions and water adsorption, the production of heat is at a maximum during the SE reaction step, far surpassing heat generation during the pressurization stage. This results in a considerable increase in the bed temperature in the case of the adiabatic reactor configuration and significant production of heat in the quasi-isothermal reactor configuration.

In order to facilitate time-efficient regeneration of the adsorbent, a depressurization step is needed to decrease the reactor pressure before the actual adsorbent regeneration. Lower reactor pressure during the adsorbent regeneration enables more efficient water desorption. It has been reported that without additional heat supply, even slightly elevated reactor pressure of several bars can have a significant adverse effect on the adsorbent regeneration rate (van Kampen et al., 2020). Therefore, it was decided to depressurize the reactor to ambient pressure before the adsorbent regeneration is commenced, as higher pressure would significantly extend the regeneration step duration. As a result of the pressure decrease and consequent water desorption, the bed temperature slightly decreases in the adiabatic reactor configuration, while a minor supply of additional heat is needed to maintain the required process temperature in the quasi-isothermal reactor configuration.

During the adsorbent regeneration step, the reactor is purged with a stream of pure nitrogen to remove water from the adsorbent and prepare the catalyst-adsorbent mixture for the next process cycle. The inlet temperature of the nitrogen stream is equal to the reactor temperature during the reaction step. The desorbed water is entrained by the nitrogen stream and removed from the reactor to be condensed in a flash separation unit operating under ambient conditions. The desorption of water from the adsorbent consumes a considerable amount of heat, which results in a significant reduction of the bed temperature in the adiabatic reactor and high heat supply demand in the quasi-isothermal reactor.

2.2. SE methanol synthesis reactor model

Details of the SE methanol synthesis reactor model were reported in our previous work (Maksimov et al., 2021), for which reason only a brief description is provided here. The pseudo-homogenous reactor model is developed based on the following assumptions: the flow can be described by an axial-dispersed plug flow model; the gradients of concentrations, pressure, velocity and temperature are considered negligible in the radial direction; neither catalyst nor adsorbent undergo deactivation; the ideal gas law is followed; and the frictional pressure drop along the catalyst-adsorbent mixture can be evaluated with Darcy's equation.

Although the 1-D assumption might seem unsubstantiated in the case of the adiabatic reactor configuration, it is crucial to ensure the computational feasibility of the current study. More specifically, as the model describes complex and rapidly changing phenomena, it requires considerable computational resources even without accounting for the radial profile. Insignificant radial dispersion can be justified by low gas flow velocities (Tsotsas and

Table 2
Conservation equations of the SE methanol synthesis reactor model.

Species mass conservation ($i \neq H_2O$)	$\frac{\partial y_i}{\partial t} = \frac{y_i}{T}\frac{\partial T}{\partial t} - \frac{y_i}{p}\frac{\partial p}{\partial t} + D_l\frac{\varepsilon_b}{\varepsilon_t}\frac{T}{p}\frac{\partial}{\partial z}\left(\frac{p\partial y_i}{T\partial z}\right) - \frac{\varepsilon_b}{\varepsilon_t}\frac{T}{p}\frac{\partial}{\partial z}\left(\frac{y_i vp}{T}\right) - \frac{\rho_{cat}RT}{\varepsilon_t p}\sum_{j\in R}\vartheta_{ij}\eta_j\left(-R_j\right)$	(4)
Water species mass conservation ($i = H_2O$)	$\frac{\partial y_{H_2O}}{\partial t} = \frac{y_{H_2O}}{T}\frac{\partial T}{\partial t} - \frac{y_{H_2O}}{p}\frac{\partial p}{\partial t} + D_l\frac{\varepsilon_b}{\varepsilon_t}\frac{T}{p}\frac{\partial}{\partial z}\left(\frac{p\partial y_{H_2O}}{T\partial z}\right) - \frac{\varepsilon_b}{\varepsilon_t}\frac{T}{p}\frac{\partial}{\partial z}\left(\frac{y_{H_2O} vp}{T}\right) - \frac{\rho_{cat}RT}{\varepsilon_t p}\sum_{j\in R}\vartheta_{H_2O,j}\eta_k\left(-R_j\right) - \frac{\rho_{ads}RT}{\varepsilon_t p}\frac{\partial q_{H_2O}}{\partial t}$	(5)
Overall mass conservation	$\frac{\partial p}{\partial t} = \frac{p}{T}\frac{\partial T}{\partial t} - \frac{\varepsilon_b T}{\varepsilon_t}\frac{\partial}{\partial z}\left(\frac{vp}{T}\right) - \frac{\rho_{cat}RT}{\varepsilon_t}\sum_{i\in I}\sum_{j\in R}\vartheta_{i,j}\eta_j\left(-R_j\right) - \frac{\rho_{ads}RT}{\varepsilon_t}\frac{\partial q_{H_2O}}{\partial t}$	(6)
Momentum conservation	$-\frac{\partial p}{\partial z} = \frac{150}{4r_p^2}\left(\frac{1-\varepsilon_b}{\varepsilon_b}\right)^2\mu v$	(7)
Overall energy conservation	$\left(\rho_{ads}C_{p,ads} + \rho_{cat}C_{p,cat} + \rho_{ads}C_{p,H_2O}q_{H_2O}\right)\frac{\partial T}{\partial t} = k_z\frac{\partial^2 T}{\partial z^2} - \frac{C_{p,g}\varepsilon_b}{R}\frac{\partial(vp)}{\partial z} + \rho_{ads}\left(-\Delta H_{ads,H_2O}\right)\frac{\partial q_{H_2O}}{\partial t} + \rho_{cat}\sum_{j\in R}\eta_j R_j\left(-\Delta H_{R,j}\right) - \frac{2h_{in}}{r_{in}}\left(T - T_w\right)$	(8)
Reactor wall element equation (Quasi-isothermal reactor)	$\rho_w C_{p,w}\frac{\partial T_w}{\partial t} = k_w\frac{\partial^2 T_w}{\partial z^2} + \frac{2r_{in}h_{in}(T-T_w)}{(r_{out}^2 - r_{in}^2)} - \frac{2r_{out}h_{out}(T_w - T_{out})}{(r_{out}^2 - r_{in}^2)}$	(9)
Reactor wall element equation (Adiabatic reactor)	$\rho_w C_{p,w}\frac{\partial T_w}{\partial t} = k_w\frac{\partial^2 T_w}{\partial z^2} + \frac{2r_{in}h_{in}(T-T_w)}{(r_{out}^2 - r_{in}^2)}$	(10)

Schlünder, 1988) due to high reactor pressure and low GHSV values, generally required for SE processes (Skorikova et al., 2020; Guffanti et al., 2021). Additionally, as reported by Guffanti et al. (Guffanti et al., 2021), dilution of the catalyst bed with adsorbent decreases the local maximum bed temperatures. Therefore, regardless of the relatively low height-to-diameter ratio of the adiabatic reactor (Table 1), the 1-D pseudo-homogeneous model is sufficient for the purpose of the current study.

The conservation equations forming the basis of the SE methanol synthesis reactor model were taken from the literature (Arora et al., 2018; Xiu et al., 2002) and adjusted in accordance with the reactor configurations investigated in this work. The conservation equations are reported in Table 2. The obtained system of PDEs is then discretized in the spatial domain into a system of coupled ODEs using the finite difference method, and solved in MATLAB using a standard integration subroutine for stiff problems – ode15s (Vande Wouwer et al., 2014). The reactor was discretized into 40 spatial compartments as practically no changes in the process performance were observed with more refined discretization.

Kinetics of water adsorption onto the employed adsorbent is described with the linear driving force model pertaining to the following equation:

$$\frac{\partial q}{\partial t} = k_{LDF}(q^* - q) \tag{11}$$

where q is the adsorbent loading, mol/kg; k_{LDF} is the mass transfer coefficient s^{-1}; and q^* is the equilibrium adsorbent loading, mol/kg.

The mass transfer coefficient in Eq. (11) accounts for micro- and macropore diffusion as well as film diffusion phenomena. The coefficient is evaluated as follows (Lin et al., 2014):

$$\frac{1}{k_{LDF}} = \left(\frac{r_p}{3k_f} + \frac{{r_p}^2}{15D_p}\right)\frac{q\rho_{ads,p}RT}{y_{H_2O}p} + \frac{{r_c}^2}{15D_c} \tag{12}$$

where: r_p – particle radius, m; k_f – film mass transfer coefficient, s^{-1}; D_p – macropore diffusivity, m^2/s; $\rho_{ads,p}$ – adsorbent particle density, kg/m^3; R – universal gas constant, J/(mol K); T – bed temperature, K; y_{H_2O} – water molar fraction; p – reactor pressure, Pa; r_c – micropore radius, m; and D_c – micropore diffusivity, m^2/s.

The equilibrium adsorbent loading value in Eq. (11) is estimated with a single-site Langmuir adsorption isotherm model according to the following equation:

$$q^* = \frac{m_{H_2O}b_{H_2O}y_{H_2O}p}{1 + b_{H_2O}y_{H_2O}p} \tag{13}$$

where m_{H_2O} is the adsorbent saturation capacity, mol/kg; and b_{H_2O} is the Langmuir adsorption isotherm parameter, Pa^{-1}.

The Langmuir adsorption isotherm parameter b_{H_2O} depends on the process temperature according to Arrhenius equation in the following manner:

$$b_{H_2O} = b_{H_2O,0}exp\left[-\frac{\Delta H_{ads,H_2O}}{RT}\right] \tag{14}$$

where: $b_{H_2O,0}$ is a Langmuir adsorption isotherm fitting parameter, Pa^{-1}; and $\Delta H_{ads,H_2O}$ is the heat of water adsorption onto the 3 Å molecular sieves, J/mol.

In our previous works (Maksimov et al., 2021; Maksimov et al., 2020), the kinetics of methanol formation were determined to be most accurately described by the kinetic interpretation proposed by Graaf et al. (Graaf et al., 1988; Graaf et al., 1986). Therefore, this kinetic model was applied to estimate the rates of the occurring chemical reactions within the scope of this work. Consequently, the kinetic expressions used to estimate the rate of the reactions, Eqs. (1)–(3), are given by Eqs. (15)–(17) respectively:

$$R_1 = \frac{k_1K_{CO}\left[f_{CO}\sqrt{{f_{H_2}}^3} - \frac{f_{CH_3OH}}{\sqrt{{f_{H_2}}^3}K_{p,1}}\right]}{\left(1 + K_{CO}f_{CO} + K_{CO_2}f_{CO_2}\right)\left[\sqrt{f_{H_2}} + \frac{K_{H_2O}}{\sqrt{K_{H_2}}}f_{H_2O}\right]} \tag{15}$$

$$R_2 = \frac{k_2K_{CO_2}\left[f_{CO_2}f_{H_2} - \frac{f_{H_2O}f_{CO}}{K_{p,2}}\right]}{\left(1 + K_{CO}f_{CO} + K_{CO_2}f_{CO_2}\right)\left[\sqrt{f_{H_2}} + \frac{K_{H_2O}}{\sqrt{K_{H_2}}}f_{H_2O}\right]} \tag{16}$$

$$R_3 = \frac{k_3K_{CO_2}\left[f_{CO_2}\sqrt{{f_{H_2}}^3} - \frac{f_{CH_3OH}f_{H_2O}}{\sqrt{{f_{H_2}}^3}K_{p,3}}\right]}{\left(1 + K_{CO}f_{CO} + K_{CO_2}f_{CO_2}\right)\left[\sqrt{f_{H_2}} + \frac{K_{H_2O}}{\sqrt{K_{H_2}}}f_{H_2O}\right]} \tag{17}$$

where R_1, R_2 and R_3 are the reaction rates per weight of catalyst for reactions (1)–(3) respectively, mol/(s kg_{cat}); k_1, k_2 and k_3 are the kinetic constants, mol/(s bar kg_{cat}); $K_{p,1}$, $K_{p,2}$ and $K_{p,3}$ are the equilibrium constants; f_i is the partial fugacity of a component i, bar; and K_i is the adsorption constant of a component i onto the catalyst surface, bar^{-1}.

The equilibrium constants in Eqs. (15)–(17) were estimated according to the correlations proposed in the latest reassessment of chemical equilibria in methanol synthesis by Graaf et al. (Graaf and Winkelman, 2016). The values of the kinetic and adsorption constants for Eqs. (15)–(17) as well as the values of the adsorbent saturation capacity and Langmuir adsorption isotherm parameter for Eqs. (13)–(14) are taken from our previous work (Maksimov et al., 2021). The mass transfer limitations affecting the rates of the occurring chemical reactions are considered through effectiveness factors in Eqs. 4–6. The values of these effectiveness factors are estimated by calculation of the Thiele modulus using the methodology developed and validated by Lommerts et al. (Lommerts et al., 2000).

2.3. Adsorbent regeneration via PSA

The complete pressure swing cycle is simulated by consecutively running the reactor model with boundary conditions adjusted for each process step (pressurization / reaction / depressurization / regeneration). At the end of each step, the gas phase composition, adsorbent loading, reactor pressure and temperature, as well as reactor wall temperature are stored and used as initial conditions for simulation of the next process step. Since the methanol synthesis reactions (Eqs. (1)–(3)) and water adsorption occur already during the pressurization step, the complete cycle simulation starts with this step. This arrangement provides an opportunity to accurately estimate saturation of the adsorbent before the reaction step is commenced.

Initial conditions for simulation of the complete process cycle are as follows: at $t = 0$,

$q = 0$, $p = p_l$ $T_r = T_{reac}$, $T_w = T_{reac}$, $y_{CO_2} = 0.25$, $y_{H_2} = 0.75$, and $y_{CO}/y_{MeOH}/y_{H_2O} = 0$. Boundary conditions for each step are provided in the **Supporting Information**.

For computational efficiency, the cyclic steady state is assumed to be achieved after the 3rd process cycle as after this point the changes in the reactor performance were observed to be practically negligible. Simulation of further process cycles would not yield any meaningful information in the context of the current work but only drastically increase the computational demands of the model, making the optimization study unfeasible.

2.4. Product separation and recirculation modeling

Modeling of the flash separation units was based on solving the Rachford-Rice equation (Finlayson, 2006). To calculate the vapor–liquid phase equilibrium, the phi-phi method was employed for updating the values of the phase equilibrium constants (Akberov, 2011). The values of fugacity coefficients and compressibility factors were estimated with the Soave-Redlich-Kwong equation of state (Soave, 1972) considering van der Waals mixing rules (Sanni, 2018). A residence time of 5 min was assumed (Skorikova et al., 2020).

To model the recirculation of the non-condensables from the high-pressure flash separation unit during the reaction step, the concentrations of each component at the reactor inlet, $y_{i,inlet}$, are consecutively adjusted considering the recirculation. The inlet concentration values are adjusted each second of the simulated time after the recirculation is commenced. The inlet concentration of each component is, therefore, determined as follows:

$$y_{i,inlet} = \frac{F_f y_{i,f} + F_r y_{i,r}}{F_f + F_r} \tag{18}$$

where: $y_{i,inlet}$ – concentration of component i entering the SE reactor during the reaction step; F_f – flowrate of the make-up stream during the reaction step, mol/s; $y_{i,f}$ – concentration of component i in the make-up stream; F_r – flowrate of the recycle stream during the reaction step, mol/s; and $y_{i,r}$ – concentration of component i in the recycle stream;

Thus, when simulating the SE reaction step, the system of coupled ODEs is integrated consecutively for each second of the reaction step. That is, the integration routine is called for each second of the reaction step separately. The interval of one second was selected as a reasonable trade-off between improved temporal resolution of the simulated phenomena and higher computational load of the model. More specifically, shortening the interval proved to drastically increase the simulation running time, while incrementing the interval resulted in coarse concentration and temperature profiles. The intermediate points, obtained during a separate integration, are discarded and only the final solution, representing the state of the reactor after the simulated second, is stored. Particularly, the stored data include the distributions of the components' concentrations, bed and wall temperatures, pressure, and adsorbent loading along the reactor length. These stored data together with the adjusted values of the inlet concentrations of the components (Eq. (18)) are then used to set the initial conditions for the subsequent integration. A visual representation of the recirculation modeling algorithm is provided in a form of a block diagram in Fig. 2. This process of stepwise consecutive integration is continued until the simulation of the reaction step is stopped.

3. Results and discussion

During the reaction step, the concentration of methanol in the reactor outlet is much higher than in conventional methanol synthesis, while the concentration of water is very low. More specifically, following the kinetic model and equilibrium constants of Graaf et al. (Graaf et al., 1988; Graaf and Winkelman, 2016); methanol and water concentrations reach respectively 6.1 mol.% and 7.1 mol.% at 50 bar and 220 °C in a conventional isothermal reactor. Similar concentration values are estimated with kinetic models of Vanden Bussche and Froment (Bussche and Froment, 1996), and Nestler et al. (Nestler et al., 2020; Nestler et al., 2021). On the other hand, at the same process conditions, in the quasi-isothermal SE methanol synthesis reactor, methanol concentration increases above 30 mol.%. At the same time, concentration of water in the reactor outlet is below 0.5 mol.%.

As the reaction step proceeds and the adsorbent is being saturated, the outlet concentration of methanol decreases, whereas the outlet concentration of water increases. In contrast to lab-scale experiments (Maksimov et al., 2021), the outlet concentration of water in the very beginning of the reaction step is not negligible. Since the adsorbent particle size is much larger compared with the laboratory experiments, the rate of water adsorption is considerably decreased. Therefore, at the end of the pressurization step, the water formed at the end of the reactor is not completely adsorbed. Consequently, as can be noted in Fig. 3, concentration of water in the reactor outlet is above zero immediately after the reaction step is commenced. Concentrations of methanol and water in the bottom product of the low-pressure flash separation unit follow the same pattern. It is worth noting that since methanol and water are the only condensable species at standard temperature and pressure, the liquid product obtained after the flash separation consists almost entirely of methanol as water is retained by the adsorbent.

The changes in the average reactor temperature for the investigated reactor configurations are vastly different. As shown in Fig. 4, the temperature in the adiabatic reactor increases drastically during the reaction step as a result of the exothermicity of the reactions and water adsorption. This increase in temperature has a detrimental effect on the adsorbent saturation capacity (Fig. 5), thus making the process less efficient in terms of water uptake. However, the excessive heat produced during the reaction step facilitates water desorption during the adsorbent regeneration step. The increase in the reactor bed temperature is sufficient to provide heat for regeneration without supplying additional heat, with the present assumption that the inlet temperature of the nitrogen purge equals the reactor feed temperature during the reaction step.

On the other hand, in the quasi-isothermal reactor, the temperature fluctuations are much less significant, and, as a consequence, much higher adsorbent saturation is achieved during the reaction step. As the tube diameter and wall thickness are comparatively large, the heat transfer between the catalyst-adsorbent bed and the boiling water in the reactor shell-side is less efficient. At the beginning of the reaction step, the temperature goes through a maximum due to the high rate of heat production in the bed. At the beginning of the regeneration step, however, the bed temperature experiences a sharp drop due to the rapid endothermic water desorption.

3.1. Methanol production rate

To investigate performance of SE methanol synthesis in terms of both improved methanol production as well as increased product purity, the process was studied so that the reaction step is stopped once the SE phase ends, i.e., before the water breakthrough point is reached. The SE phase duration depends on the adsorbent saturation. However, as illustrated in Fig. 3, with the given process configuration, the concentration of water increases gradually. Consequently, isolating a single point, signifying a distinctive end of the SE phase, while maintaining a reasonably low water concentration in the product is not possible. Therefore, the reaction step was stopped when the concentration of methanol in the blend methanol product drops below 95 wt%.

Since adsorbent loading during the regeneration step decreases exponentially (Fig. 5), completely regenerating the adsorbent would be counterproductive in terms of average methanol production rate. However, the adsorbent should be regenerated sufficiently so that the process performance and product purity are maintained at a reasonably high level during the subsequent process cycles. Particularly, if the blend product purity is maintained above 95 wt%, the amount of methanol obtained during a single cycle was found to decrease by ca. 6.5 % on average if the adsorbent

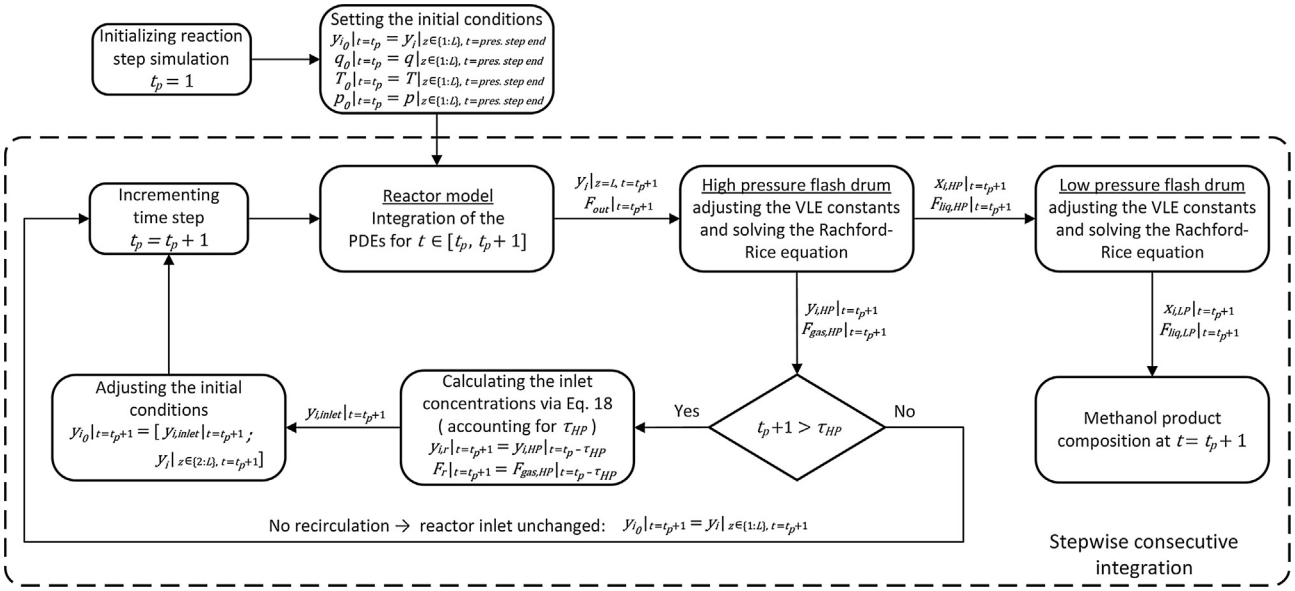

Fig. 2. Block diagram of the algorithm for reaction step simulation t_p – time step during the reaction step simulation, s; F_{out} – flowrate of the reactor outlet stream during the reaction step, mol/s; $F_{gas,HP}$ and $F_{liq,HP}$ – flowrate of the top and bottom products of the high-pressure flash drum, respectively, mol/s; $x_{i,HP}$ and $y_{i,HP}$ – component molar fraction in the bottom and top products of the high-pressure flash drum, respectively; $F_{liq,LP}$ – flowrate of the bottom product of the low-pressure flash drum, mol/s; $x_{i,LP}$ - component molar fraction in the bottom product of the low-pressure flash drum.

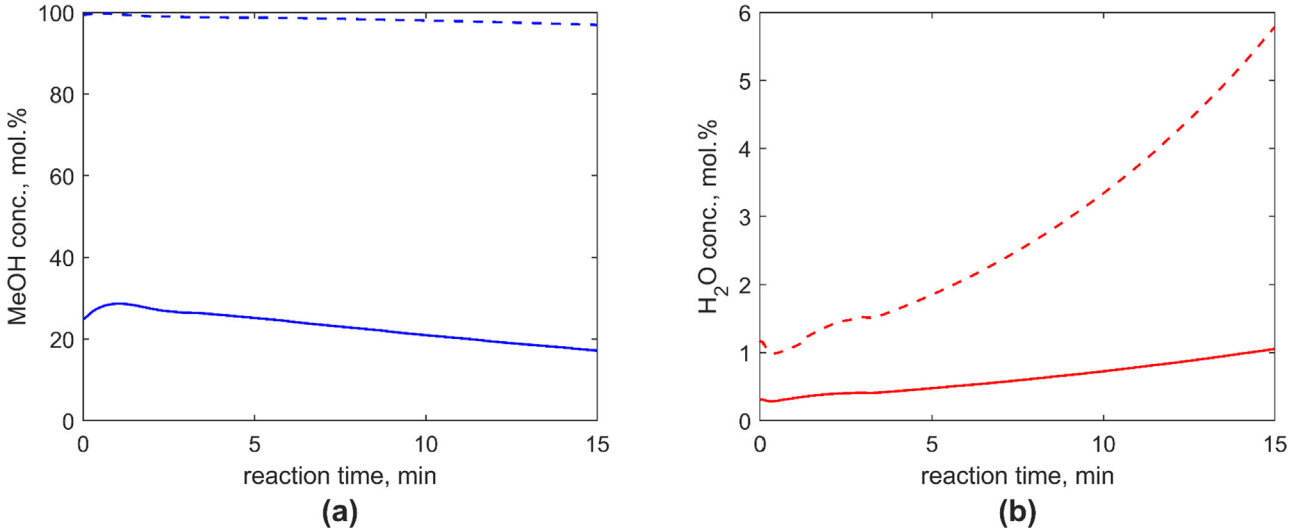

Fig. 3. Simulated evolution of methanol (a) and water (b) concentrations during the reaction step; quasi-isothermal reactor configuration; catalyst:adsorbent ratio – 1:1; temperature – 220 °C; GHSV – 400 h^{-1}; solid lines denote values at the reactor outlet; dashed lines denote values in the bottom product of the low-pressure flash drum (the values are shifted in time accounting for the flow residence time in the separation section).

loading after the regeneration step is kept at 5% of the maximum attainable loading for given process conditions. For the values of 10 %, 20 %, and 50 % of the maximum attainable loading, the decrease is ca. 12.9 %, 26.5 %, and 75.8 % respectively. Therefore, the regeneration step was considered complete when the average adsorbent loading in the reactor drops below 5% of the average adsorbent loading at the end of the reaction step.

The specific methanol production rate over a complete process cycle is, therefore, determined as:

$$\text{Prod}_{MeOH} = \frac{\left(\int_{t_{start}}^{t_{end}} x_{MeOH,LP} F_{LP} \mathrm{d}t\right) MW_{MeOH}}{t_{cycle} V_r} \tag{19}$$

where:

Prod_{MeOH} – specific methanol production rate, kg/(m^3 min); $x_{MeOH,LP}$ – methanol concentration in the bottom product of the low-pressure flash drum; F_{LP} – molar flowrate of the bottom product of the low-pressure flash drum, mol/s; MW_{MeOH} – methanol molar weight, kg/mol; t_{cycle} – total cycle duration, min; V_r – reactor volume, m^3; t_{start} – time, when the reaction step is commenced, s; and t_{end} – time, when the reaction step is stopped, s.

The combined effect of the catalyst-adsorbent ratio and process temperature is of great interest, as these parameters largely determine the water retention capabilities of the reactor and, consequently, the duration and efficiency of the SE phase. Therefore, a parametric study investigating the specific methanol production rate (Eq. (19)) in a SE methanol synthesis reactor at different process temperatures with varying bed composition was conducted

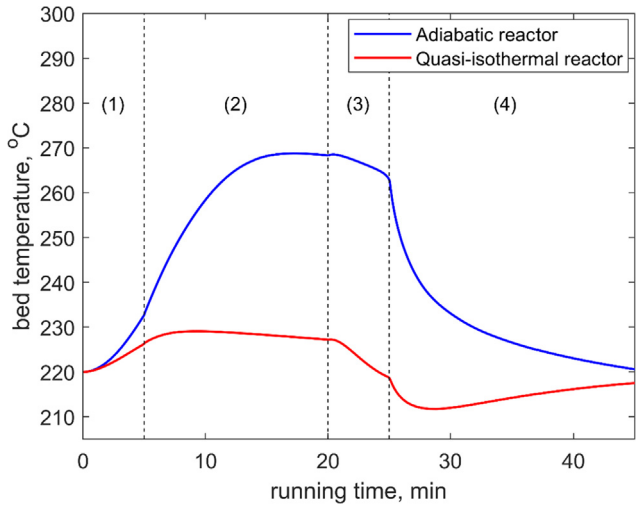

Fig. 4. Simulated evolution of the average reactor temperature for the investigated reactor configurations; catalyst:adsorbent ratio – 1:1; temperature – 220 °C; GHSV – 400 h^{-1}; (1) – pressurization; (2) – reaction; (3) – depressurization; (4) – regeneration.

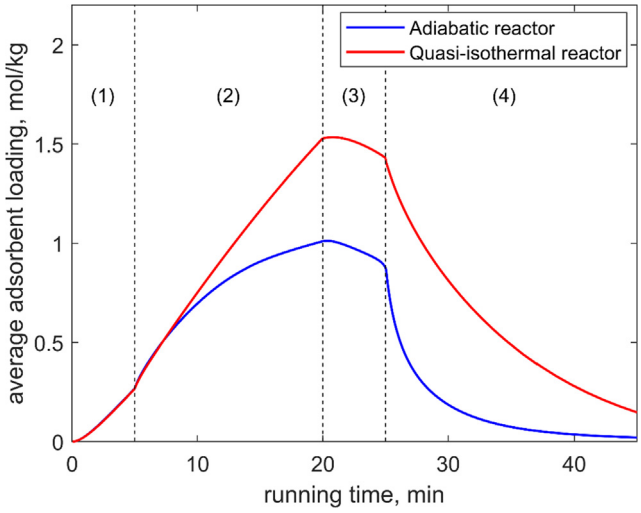

Fig. 5. Simulated evolution of the average adsorbent loading for the investigated reactor configurations; catalyst:adsorbent ratio – 1:1; temperature – 220 °C; GHSV – 400 h^{-1}; (1) – pressurization; (2) – reaction; (3) – depressurization; (4) – regeneration.

for GHSV of 200, 400 and 800 h^{-1} referring to the whole bed volume. The GHSV range was selected to ensure feasible duration of the reaction step within the limits of 5 and 120 min. The range is in good agreement with the values previously reported for SE DME synthesis studies (Skorikova et al., 2020; Guffanti et al., 2021). The results are given in Fig. 6 and Table 3.

It can be noted that a clear optimal combination of process temperature and catalyst-adsorbent ratio exists for each case. Moreover, an increase in GHSV results in consistent methanol production rate improvement, although at the cost of moderately narrowing the optimal parameters envelope. The increase in production rate is achieved as a result of shortening both the reaction and regeneration steps. In general, the results agree reasonably well with the findings of Arora et al. (Arora et al., 2018). However, the results obtained in this work provide optimal process parameters that ensure production of high purity methanol product, which significantly simplifies downstream processing.

In general, increasing the GHSV results in an increase in the optimal reactor temperature as this improves the kinetics of the occurring reactions. This shift of the optimal reactor temperature is more prominent in the quasi-isothermal reactor since temperature control is more efficient with this configuration. In contrast, overheating during the reaction step in the adiabatic reactor is significant already at the optimal temperature, which evidently hinders methanol production. Consequently, the methanol production rate is generally ca. 30% lower in the adiabatic reactor configuration. It is also worth noting that the ratio of the reaction step duration to the regeneration step duration decreases with increasing GHSV. This ratio is more favorable for the quasi-isothermal reactor configuration in light of the more efficient temperature control. In general, even for the high GHSV value, the steps are comparable in terms of duration.

Furthermore, in addition to the analysis of the specific production rate, methanol yield was investigated in order to evaluate the loss of the reactant and product species due to the depressurization and purging steps and the low-pressure flash separation. Methanol yield values were determined for both reactor configurations for different process temperatures at varying bed composition. The results can be found in the **Supporting Information**. It is noteworthy that methanol yields are below 90% regardless of complete recirculation of the non-condensables during the reaction step. The cause for the low yields is the losses of methanol during the depressurization and purging steps. In the current design, methanol removed from the reactor during these steps is not collected as a product but is instead combusted to acquire additional heat. However, it should be emphasized that the process is not optimized, and the losses can be reduced with additional recirculation loops and separation units. The highest yields were recorded close to the optimal catalyst:adsorbent ratios for the highest specific methanol production rates.

3.2. Guard layer configuration

One way of increasing the purity of the obtained methanol product is to substitute the catalyst-adsorbent mixture at the end of the reactor with pure adsorbent. Such a configuration would ensure that the reactor outlet stream at the beginning of the reaction step contains a minimum amount of water. The adsorbent layer at the end of the reactor is thus termed the *guard layer*. As presented in Fig. 7, incorporating a guard layer in the SE reactor provides an opportunity to considerably decrease water concentration in the outlet stream and in the obtained methanol product. However, it is also worth noting that the methanol production rate is slightly lower since the total amount of catalyst in the SE reactor with the guard layer is lower than in a conventional SE reactor at the same catalyst-adsorbent ratio.

The performance of the SE reactors with a guard layer was evaluated in terms of the specific methanol production rate following the methodology and constraints outlined in the previous section. The guard layer volume for the investigated cases is taken as 10% and 20% of the total reactor volume. The parametric study results are given in Fig. 8 and Table 4.

The results of the parametric study indicate that introducing a guard layer in a SE methanol synthesis reactor causes a marginal decrease in the specific production rate even with optimal process parameters. This decrease is more significant in the case of the adiabatic reactor configuration due to the less favorable conditions for water adsorption. The decrease in the production rate depends on the guard layer volume, as the increase in the guard layer thickness is inversely proportional to the total amount of catalyst in the reactor. Therefore, although the estimated optima are practically unchanged relative to the conventional SE reactor configuration, increasing the guard layer volume to 20% in the case of the

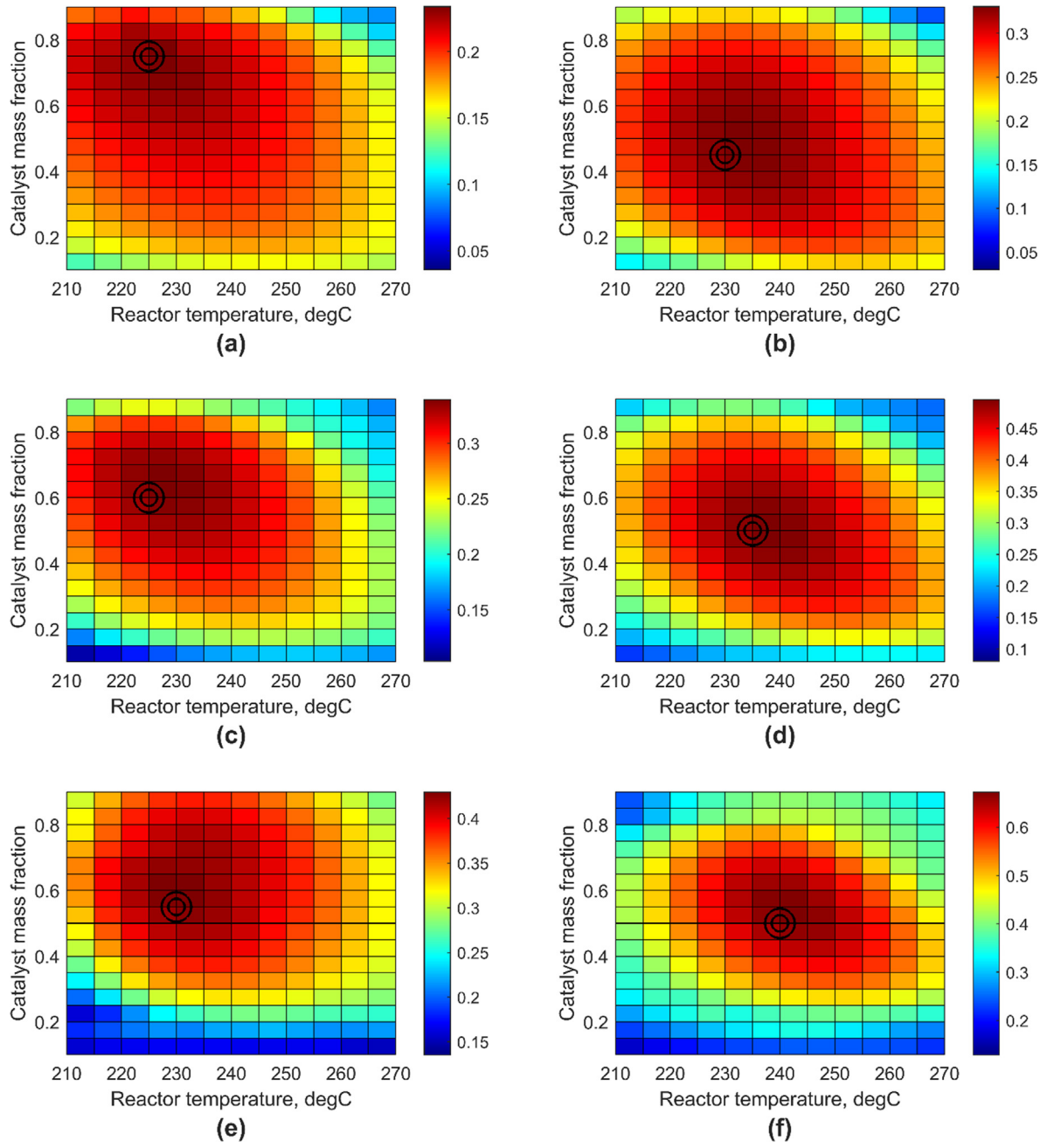

Fig. 6. Specific methanol production rate as a function of process temperature and bed composition; the color bars represent specific methanol production rate, kg/(m^3 min); (a), (c), (e) – results for the adiabatic reactor configuration for 200, 400 and 800 h^{-1} respectively; (b), (d), (f) – results for the quasi-isothermal reactor configuration for 200, 400 and 800 h^{-1} respectively; the mark with 2 concentric circles denotes the point of maximum methanol production rate.

Table 3
Optimal values of process temperature and catalyst mass fraction for SE methanol synthesis.

	Adiabatic reactor configuration			Quasi-isothermal reactor configuration		
GHSV, h^{-1}	200	400	800	200	400	800
Temperature, ºC	225	225	230	230	235	240
Catalyst fraction (mass basis)	0.75	0.60	0.55	0.45	0.50	0.50
Specific methanol production rate, kg/(m^3 min)	0.23	0.36	0.43	0.33	0.49	0.67
Reaction step duration, min	19.9	11.9	5.7	68.2	29.8	12.5
Regeneration step duration, min	15.2	10.9	6.6	31.8	18.5	8.5

quasi-isothermal reactor shifts the optimal catalyst fraction in the bed toward the higher values. This effect is less pronounced for the adiabatic reactor due to its generally much lower productivity.

The results of the parametric study investigating methanol yield in the SE reactors with the guard adsorbent layer can be found in the **Supporting Information**. It can be concluded that introduction

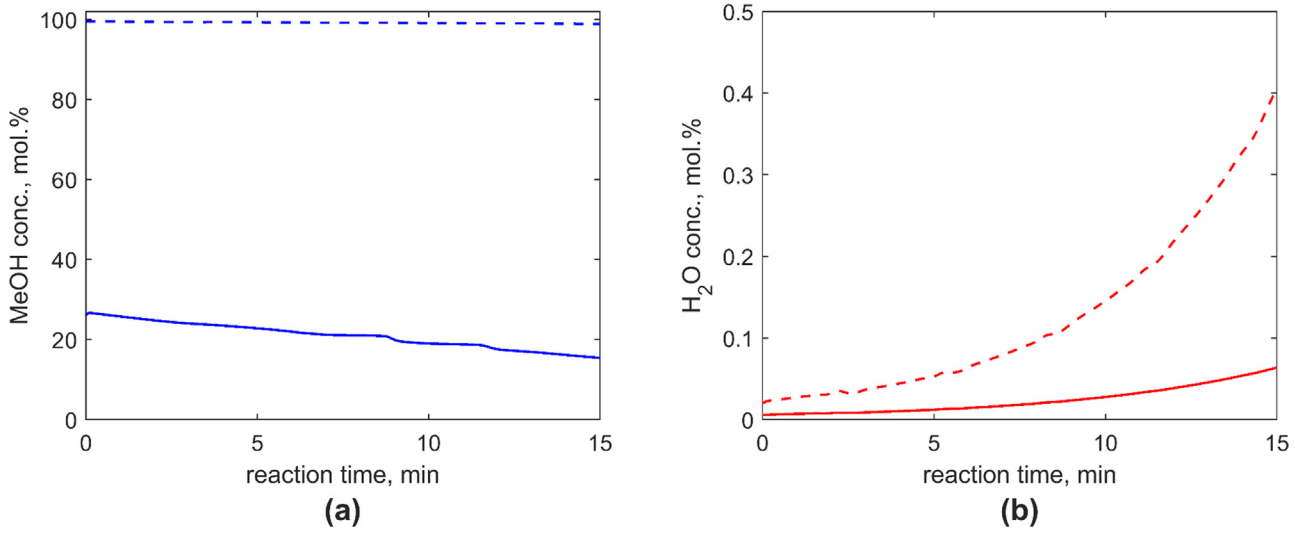

Fig. 7. Simulated evolution of methanol (a) and water (b) concentrations in the SE reactor with guard layer during the reaction step; quasi-isothermal reactor configuration; catalyst-adsorbent ratio – 1:1; temperature – 220 °C; GHSV – 400 h^{-1}; guard layer volume – 10% of the total reactor volume; solid lines denote values at the reactor outlet; dashed lines denote values in the bottom product of the low-pressure flash drum (the values are shifted in time accounting for the flow residence time in the separation section).

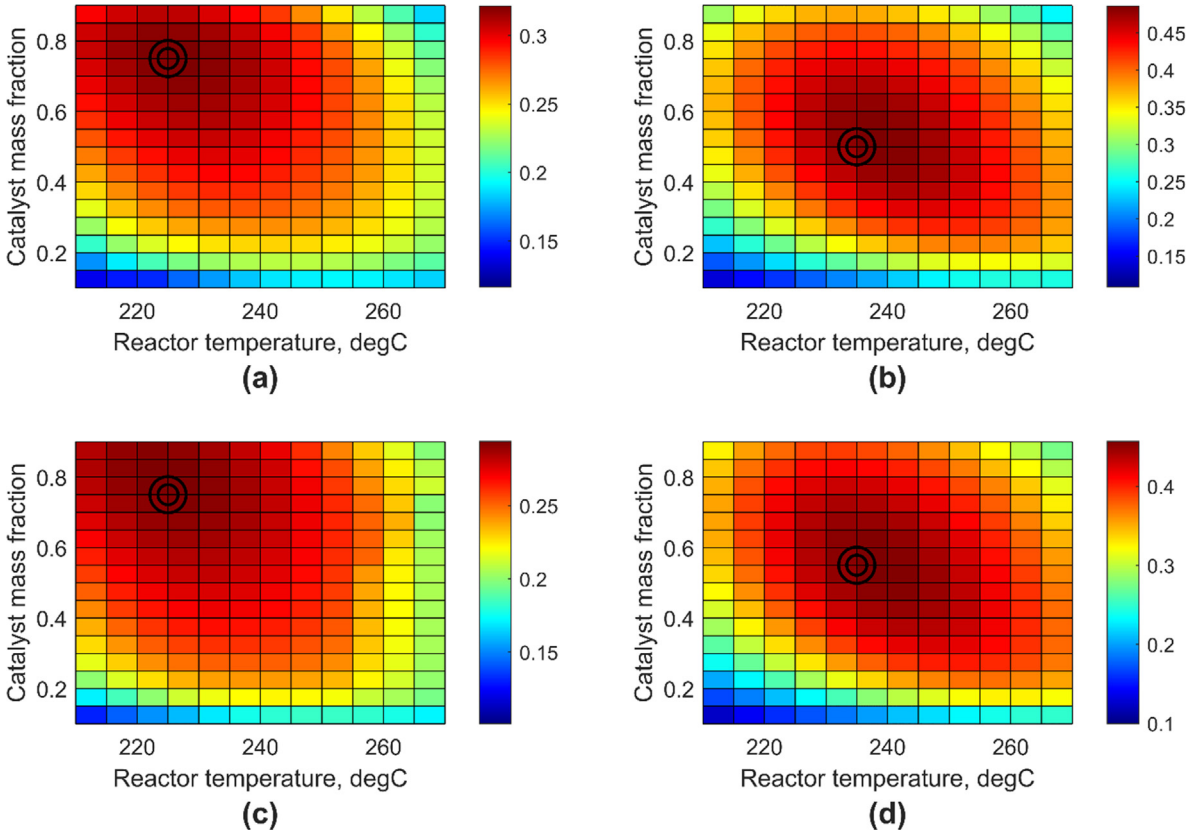

Fig. 8. Specific methanol production rate as a function of process temperature and bed composition in the SE reactors with guard layer; the color bars represent specific methanol production rate, kg/(m^3 min); (a) – the adiabatic reactor configuration with 10% guard layer; (b) – the quasi-isothermal reactor configuration with 10% guard layer; (c) – the adiabatic reactor configuration with 20% guard layer; (d) – the quasi-isothermal reactor configuration with 20% guard layer; the mark with 2 concentric circles denotes the point of maximum methanol production rate.

of the guard layer does not substantially affect methanol yield. However, it is worth noting that the pattern of the increase in the optimal catalyst fraction with the increase in the guard layer volume is also relevant for the methanol yield values.

3.3. Methanol product purity vs production rate

Improving the methanol production rate and increasing the obtained methanol product purity are conflicting objectives as an

Table 4
Optimal values of process temperature and catalyst mass fraction for SE methanol synthesis in SE reactors with a guard layer.

	Adiabatic reactor configuration		Quasi-isothermal reactor configuration	
Guard layer, fraction of the total reactor volume	10 %	20 %	10 %	20 %
GHSV, h^{-1}	400	400	400	400
Temperature, °C	225	225	235	235
Catalyst fraction (mass basis)	0.75	0.75	0.50	0.55
Specific methanol production rate, kg/(m^3 min)	0.32	0.29	0.48	0.45
Reaction step duration, min	16.3	22.8	40.5	48.5
Regeneration step duration, min	10.6	13.6	19.1	18.5

increase in one will inevitably cause a decrease in the other. Therefore, a multi-objective optimization study was performed to investigate the tradeoff between the methanol product purity and specific methanol production rate. Instead of a single optimum, multi-objective optimization yields a set of solutions among which selection of the best solution is challenging without additional input regarding preference for one of the objectives. These solutions are called non-dominated solutions. The non-dominated solutions form a front, which is often referred to as Pareto front.

The optimization study was conducted considering the following 4 process parameters: process temperature, catalyst-adsorbent ratio, GHSV and reaction step duration. The specific methanol production rate was determined following Eq. (19). Methanol product purity was expressed as methanol concentration (on a mass basis) in the final methanol product blend. To obtain a well distributed frontier of the non-dominated solutions, a non-dominated sorting genetic algorithm (NSGA-II) (Deb et al., 2002) was employed. As an evolutionary algorithm, NSGA-II is exceptionally efficient in terms of avoiding local minima, a shortcoming that is particularly significant for gradient-based optimization algorithms (Subraveti et al., 2019). In addition to that, due to its capability of preserving diversity among solutions within the same nondominated front, NSGA-II yields a well-resolved Pareto front. This way, NSGA-II is the most practical algorithm for investigating the trade-off between several conflicting objectives, as was demonstrated by previous studies on the topic of PSA processes optimization (Hao et al., 2021; Haghpanah et al., 2013).

The optimization study was performed for both reactor configurations with and without a guard adsorbent layer. Taking account of the results of the parametric studies, the guard layer volume was fixed at 10% of the total reactor volume. This value was selected as a reasonable tradeoff between the decrease in specific methanol production rate and increase in product purity.

In view of the high computational demand of the optimization problem, the maximum number of generations was limited to 20. The population size of each generation was set to 50 for the purpose of acquiring a sufficient number of optimal non-dominated solutions, thus ensuring a well resolved shape of the Pareto front. Although the maximum number of generations may seem low, the obtained results indicate that the intermediate solutions oscillate in close vicinity to the non-dominated solutions in the final generations. Therefore, further increase in the number of maximum generations would not be worth the additional computational effort. To ensure that the optimization is performed within the feasible region, upper and lower bounds were applied to the investigated process parameters (Table 5). The optimization algorithm was implemented in MATLAB using the '*gamultiobj*' function.

Since the current optimization study focuses solely on the methanol production rate and product purity, identifying a single optimum point among the determined non-dominated solutions is challenging. Therefore, for each set of non-dominated solutions, a single optimal solution was selected following the technique for the order of preference by similarity to the ideal solution (Wang and Rangaiah, 2017). In this optimization study, the ideal solution is a non-existent hypothetical point of maximum attainable specific methanol production rate and maximum attainable product purity. The obtained results are given in Fig. 9. The optimal process parameters determined for the non-dominated solutions are provided in the **Supporting Information**.

Table 5
Constraints for the multi-objective optimization study.

	Lower bounds	Upper bounds
Reactor temperature, °C	200	250
Catalyst mass fraction	0.2	0.8
GHSV, h^{-1}	200	1000
Reaction step duration, min	5	120

The results indicate a clear inverse relationship between the specific methanol production rate and product purity. Improving product purity requires maintaining favorable conditions for water adsorption in the SE reactor and/or stopping the reaction step earlier. Consequently, non-dominated solutions associated with increased product purity are given by lower values of reactor temperature, catalyst fraction and GHSV, as well as shorter reaction steps. On the other hand, the points of increased methanol production rate favor enhancing methanol synthesis reactions over facilitating the adsorption phenomena. Thus, higher values of GHSV and catalyst fraction are preferred for the higher specific methanol production rate, while temperature generally oscillates around the optimal point. The reaction step is also maintained for a much longer period.

In the case of the quasi-isothermal reactor configuration, the determined Pareto front follows the parabolic trend common for two-objective-maximization problems, whereas for the adiabatic reactor, the front exhibits a rather non-convex shape. In general, in agreement with the results of the parametric studies, methanol production is much less favorable for the adiabatic configuration. The Pareto fronts determined for the guard layer reactor configurations bear considerable similarities with the results acquired for the conventional SE reactors. However, it is worth noting that for the reactors with a guard adsorbent layer, higher methanol production rates are maintained at increased product purity. At the same time, the decrease in product purity with increase in specific production rate is also much steeper after the tipping point for the SE reactors with the guard adsorbent layer. Consequently, the optima estimated for the conventional SE reactors exhibit lower product purity.

Although the optima selected for the determined sets of non-dominated solutions provide general information about the process conditions most suitable for satisfying both objectives, they are dependent on the points of maximum production rate and product purity. Therefore, these selected optima might be misleading when selecting a target production rate and product purity. Hence, in the current study the acquired Pareto fronts were investigated

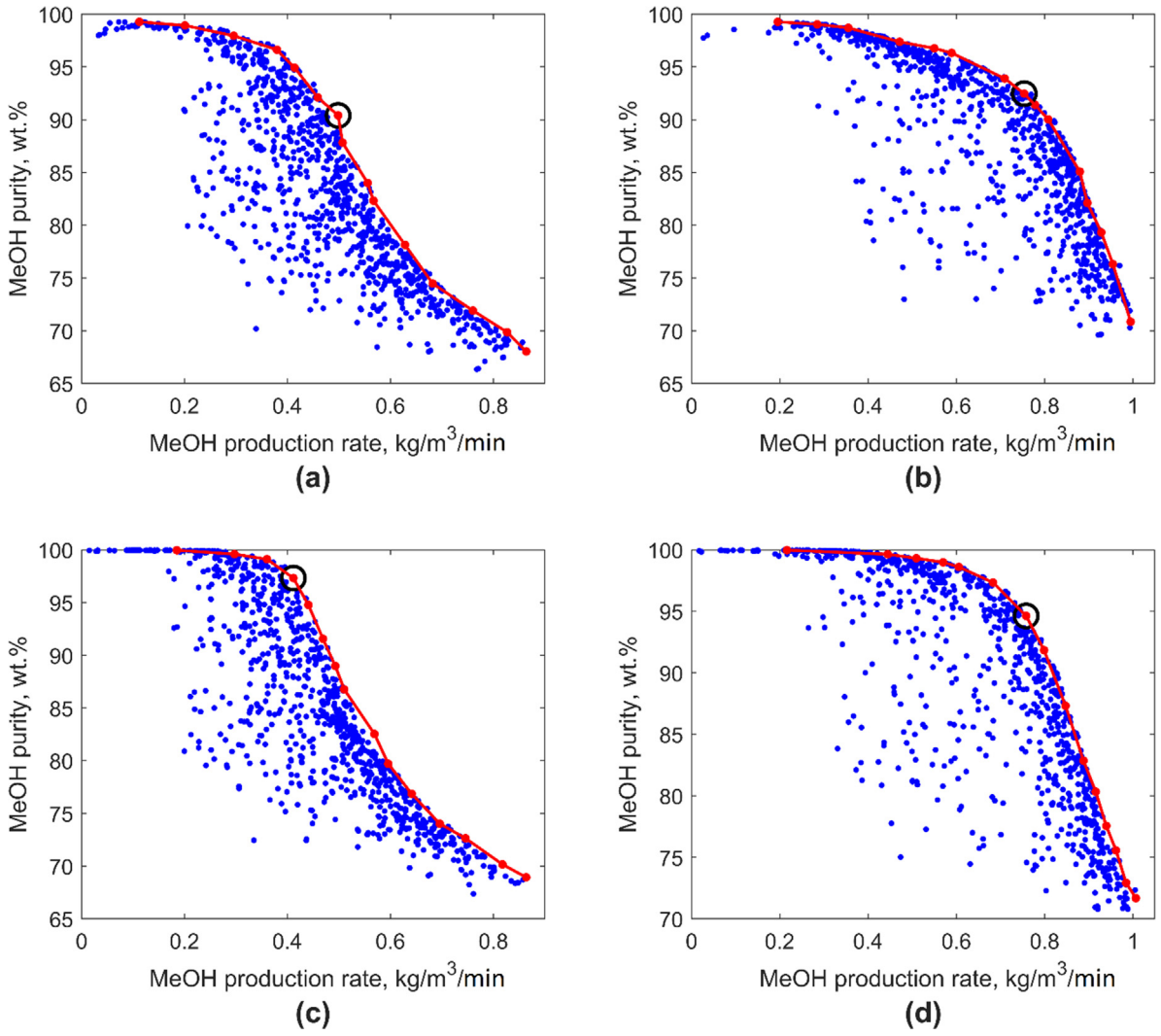

Fig. 9. Multi objective optimization results (a) – adiabatic reactor configuration; (b) – quasi-isothermal reactor configuration; (c) – adiabatic reactor configuration with 10% guard layer; (d) – quasi-isothermal reactor configuration with 10% guard layer; blue markers denote intermediate optimization results; red markers denote non-dominated solutions; black circles highlight selected numerical optimums.

further to analyze the tradeoff between the conflicting objectives. Following the approach of marginal rate substitution (Dorfman, 2017), the gain in specific methanol production rate per unit of sacrifice in the product quality was determined for the acquired non-dominated solutions. The results are given in the **Supporting Information**. Considering the obtained results, it is noteworthy that the region of highest increase in the specific production rate with the lowest decrease in the product purity is found at lower methanol production rates. This tradeoff is considerably more favorable for the reactor configurations with the guard adsorbent layer. Furthermore, in this regard, the quasi-isothermal reactor configuration is also preferable over the adiabatic configuration. Based on these results, it can be concluded that the quasi-isothermal reactor configuration with a guard adsorbent layer is the better option for production of higher purity methanol product via sorption enhanced carbon dioxide hydrogenation.

It should be noted that the optimal points highlighted by the black circles in Fig. 9 only represent numerical optimums aiming to minimize the trade-off between the methanol production rate and the product purity. In practical application, the required limit on the purity would be imposed by the intended uses of the methanol product and the resulting purity requirements. For instance, production of chemical grade methanol would require a very high purity, resulting in short duration of the reaction step to limit water breakthrough. On the other hand, the purity limit could be decreased for fuel grade methanol or when producing methanol to be further converted, depending on the requirements of the subsequent conversion processes. If highly pure methanol is required, addition of a distillation step may be required, eliminating or limiting the benefits of simplified product separation facilitated by the SE process.

Although the results of the parametric and optimization studies performed in this work provide practically useful information in terms of the optimal process parameters and their impact on the process performance, it is worth remarking that the absolute values of the specific production rate and methanol yield might be subject to moderate changes in the context of actual industrial operation. Due to very low technology readiness level, the long-term operation of an SE reactor is associated with many uncertainties. Some recent research findings (Catarina Faria et al., 2018; An et al., 2018) indicate that in-situ removal of water in an SE hydrogenation reactor might increase formation of carbonaceous species that in time could cause catalyst deactivation and decrease adsorbent performance. However, coke formation is enhanced at lower

pressures and higher temperatures (Massa et al., 2020; Peinado et al., 2020). In this regard, considering the process conditions studied in this work, the process performance is not likely to degrade significantly due to coke deposition.

4. Conclusions

Methanol production from carbon dioxide and hydrogen is severely limited by thermodynamic equilibrium. The thermodynamic limitations can be alleviated by in-situ removal of water from the reaction zone. For this purpose, a water selective adsorbent can be introduced in a methanol synthesis reactor – a process intensification strategy generally known as sorption enhanced (SE) synthesis. Although the water removal significantly improves carbon dioxide hydrogenation to methanol, the enhancement comes at the cost of a non-steady mode of operation and the need for adsorbent regeneration. Therefore, design and optimization of an SE methanol synthesis process is a multifaceted and exceedingly complex process.

In this work, the process of SE methanol synthesis was studied by means of mathematical modeling accounting for product separation and recirculation of the unreacted gases. A series of parametric and optimization studies were performed with the purpose of investigating the maximum efficiency of the SE methanol synthesis and optimal operation parameters. Both quasi-isothermal and adiabatic reactor configurations were considered as each of them possesses advantageous features in the context of the studied process. Reactor configurations with a guard adsorbent layer were proposed and investigated. Multi-objective optimization was conducted to analyze the trade-off between an increased specific methanol production rate and improved purity of the obtained product.

Optimal values of reactor temperature and catalyst-adsorbent ratio were determined for production of methanol product with limited water concentration. The results demonstrate that the specific methanol production rate depends greatly on the GHSV, which suggests that SE methanol synthesis suffers from the low flowrates generally required in such processes to ensure efficient water adsorption. Although the optimal combinations of reactor temperature and catalyst-adsorbent ratio experience slight variations at changing GHSV, the favorable reactor temperature is generally around 215 °C and 235 °C for the adiabatic and quasi-isothermal reactors respectively, while the optimal catalyst mass fraction values are ca. 0.65 and ca. 0.50 for the same reactor configurations.

The results of the multi-objective optimization study clearly demonstrate the tradeoff between the specific methanol production rate and the purity of the obtained product and highlight the importance of efficient temperature control in SE methanol synthesis. Based on this study, the quasi-isothermal reactor with a guard adsorbent layer can be considered the optimal configuration for production of higher purity methanol product. With this configuration, a product consisting almost entirely of methanol (99 wt%) can be produced at a rate of ca. 0.44–0.45 kg/min per cubic meter of total bed volume.

CRediT authorship contribution statement

Pavel Maksimov: Conceptualization, Methodology, Software, Data curation, Writing – original draft, Writing – review & editing. **Harri Nieminen:** Conceptualization, Methodology, Writing – review & editing. **Arto Laari:** Conceptualization, Methodology, Writing – review & editing, Supervision, Project administration, Funding acquisition. **Tuomas Koiranen:** Conceptualization, Methodology, Writing – review & editing, Supervision, Project administration, Funding acquisition.

Declaration of Competing Interest

The authors declare that they have no known competing financial interests or personal relationships that could have appeared to influence the work reported in this paper.

Acknowledgements:

Business Finland (Finland) is acknowledged for the main financial support of the P2XEnable project (p2xenable.fi). The project partners are also thanked for their financial contributions.

Appendix A. Supplementary material

Supplementary data to this article can be found online at https://doi.org/10.1016/j.ces.2022.117498.

References

Kung, H.H., 1994. Methanol Production and Use. Marcel Dekker, New York.
Gurau, V., Ogunleke, A., Strickland, F., 2020. Design of a methanol reformer for on-board production of hydrogen as fuel for a 3 kW High-Temperature Proton Exchange Membrane Fuel Cell power system. Int. J. Hydrogen Energy. 45, 31745–31759. https://doi.org/10.1016/j.ijhydene.2020.08.179.
Fiedler Eckhard, G. Georg, Kersebohm D. Burkhard, W. Gunther, W. Claus, Methanol, in: Ullmann'S Encycl. Ind. Chem., Wiley-VCH Verlag GmbH & Co. KGaA, Weinheim, 2007.
Kätelhön, A., Meys, R., Deutz, S., Suh, S., Bardow, A., 2019. Climate change mitigation potential of carbon capture and utilization in the chemical industry. Proc. Natl. Acad. Sci. U. S. A. 116 (23), 11187–11194. https://doi.org/10.1073/pnas.1821029116.
Westerterp, K.R., Kuczynski, M., Kamphuis, C.H.M., 1989. Synthesis of Methanol in a Reactor System with Interstage Product Removal. Ind. Eng. Chem. Res. https://doi.org/10.1021/ie00090a018.
Arena, F., Barbera, K., Italiano, G., Bonura, G., Spadaro, L., Frusteri, F., 2007. Synthesis, characterization and activity pattern of Cu-ZnO/ZrO2 catalysts in the hydrogenation of carbon dioxide to methanol. J. Catal. 249 (2), 185–194. https://doi.org/10.1016/j.jcat.2007.04.003.
Ma, J., Sun, N., Zhang, X., Zhao, N., Xiao, F., Wei, W., Sun, Y., 2009. A short review of catalysis for CO2 conversion. Catal. Today. 148 (3-4), 221–231. https://doi.org/10.1016/j.cattod.2009.08.015.
Sahibzada, M., Metcalfe, I.S., Chadwick, D., 1998. Methanol synthesis from CO/CO2/H2 over Cu/ZnO/Al2O3 at differential and finite conversions. J. Catal. 174 (2), 111–118. https://doi.org/10.1006/jcat.1998.1964.
van Kampen, J., Boon, J., van Sint Annaland, M., 2021. Separation enhanced methanol and dimethyl ether synthesis. J. Mater. Chem. A. 9, 14627–14629. https://doi.org/10.1039/d1ta03405g.
van Kampen, J., Boon, J., van Berkel, F., Vente, J., van Sint Annaland, M., 2019. Steam separation enhanced reactions: Review and outlook. Chem. Eng. J. 374, 1286–1303. https://doi.org/10.1016/j.cej.2019.06.031.
van Bennekom, J.G., Venderbosch, R.H., Winkelman, J.G.M., Wilbers, E., Assink, D., Lemmens, K.P.J., Heeres, H.J., 2013. Methanol synthesis beyond chemical equilibrium. Chem. Eng. Sci. 87, 204–208. https://doi.org/10.1016/j.ces.2012.10.013.
Reichert, J., Maerten, S., Meltzer, K., Tremel, A., Baldauf, M., Wasserscheid, P., Albert, J., 2019. Shifting the equilibrium of methanol synthesis from CO2 by: In situ absorption using ionic liquid media. Sustain. Energy Fuels. 3 (12), 3399–3405.
Bos, M.J., Brilman, D.W.F., 2015. A novel condensation reactor for efficient CO2 to methanol conversion for storage of renewable electric energy. Chem. Eng. J. 278, 527–532. https://doi.org/10.1016/j.cej.2014.10.059.
Carvill, B.T., Hufton, J.R., Anand, M., Sircar, S., 1996. Sorption-Enhanced Reaction Process. AIChE J. 42 (10), 2765–2772. https://doi.org/10.1002/aic.690421008.
Li, Z., Deng, Y., Dewangan, N., Hu, J., Wang, Z., Tan, X., Liu, S., Kawi, S., 2021. High Temperature Water Permeable Membrane Reactors for CO2 Utilization. Chem. Eng. J. 420, 129834. https://doi.org/10.1016/j.cej.2021.129834.
Sandström, L., Palomino, M., Hedlund, J., 2010. High flux zeolite X membranes. J. Memb. Sci. 354 (1-2), 171–177. https://doi.org/10.1016/j.memsci.2010.02.050.
Lee, S.M., Xu, N., Grace, J.R., Li, A., Lim, C.J., Kim, S.S., Fotovat, F., Schaadt, A., White, R. J., 2018. Structure, stability and permeation properties of NaA zeolite membranes for H2O/H2 and CH3OH/H2 separations. J. Eur. Ceram. Soc. 38 (1), 211–219. https://doi.org/10.1016/j.jeurceramsoc.2017.08.012.
Zhu, W., Gora, L., van den Berg, A.W.C., Kapteijn, F., Jansen, J.C., Moulijn, J.A., 2005. Water vapour separation from permanent gases by a zeolite-4A membrane. J. Memb. Sci. 253 (1-2), 57–66. https://doi.org/10.1016/j.memsci.2004.12.039.

Li, H., Qiu, C., Ren, S., Dong, Q., Zhang, S., Zhou, F., Liang, X., Wang, J., Li, S., Yu, M., 2020. Na + -gated water-conducting nanochannels for boosting CO 2 conversion to liquid fuels. Science 367 (6478), 667–671.
Borgschulte, A., Gallandat, N., Probst, B., Suter, R., Callini, E., Ferri, D., Arroyo, Y., Erni, R., Geerlings, H., Züttel, A., 2013. Sorption enhanced CO2 methanation. Phys. Chem. Chem. Phys. 15 (24), 9620. https://doi.org/10.1039/c3cp51408k.
J. Boon, K. Coenen, E. van Dijk, P. Cobden, F. Gallucci, M. van Sint Annaland, Sorption-Enhanced Water–Gas Shift, in: Adv. Chem. Eng., 2017. https://doi.org/10.1016/bs.ache.2017.07.004.
Hu, Y., Cui, H., Cheng, Z., Zhou, Z., 2019. Sorption-enhanced water gas shift reaction by in situ CO2 capture on an alkali metal salt-promoted MgO-CaCO3 sorbent. Chem. Eng. J. 377, 119823. https://doi.org/10.1016/j.cej.2018.08.209.
van Kampen, J., Boon, J., Vente, J., van Sint Annaland, M., 2020. Van Sint Annaland, Sorption enhanced dimethyl ether synthesis for high efficiency carbon conversion: Modelling and cycle design. J. CO2 Util. 37, 295–308. https://doi.org/10.1016/j.jcou.2019.12.021.
Van Kampen, J., Boon, J., Vente, J., Van Sint Annaland, M., 2021. Sorption enhanced dimethyl ether synthesis under industrially relevant conditions: Experimental validation of pressure swing regeneration. React. Chem. Eng. 6, 244–257. https://doi.org/10.1039/d0re00431f.
Skorikova, G., Saric, M., Sluijter, S.N., van Kampen, J., Sánchez-Martínez, C., Boon, J., 2020. The Techno-Economic Benefit of Sorption Enhancement: Evaluation of Sorption-Enhanced Dimethyl Ether Synthesis for CO2 Utilization. Front. Chem. Eng. 2. https://doi.org/10.3389/fceng.2020.594884.
Terreni, J., Trottmann, M., Franken, T., Heel, A., Borgschulte, A., 2019. Sorption-Enhanced Methanol Synthesis. Energy Technol. 7 (4), 1801093. https://doi.org/10.1002/ente.201801093.
Maksimov, P., Laari, A., Ruuskanen, V., Koiranen, T., Ahola, J., 2021. Methanol synthesis through sorption enhanced carbon dioxide hydrogenation. Chem. Eng. J. 418, 129290. https://doi.org/10.1016/j.cej.2021.129290.
Graaf, G.H., Stamhuis, E.J., Beenackers, A.A.C.M., 1988. Kinetics of low-pressure methanol synthesis. Chem. Eng. Sci. 43 (12), 3185–3195. https://doi.org/10.1016/0009-2509(88)85127-3.
Nikolic, M., Daemen, L., Ramirez-Cuesta, A.J., Xicohtencatl, R.B., Cheng, Y., Putnam, S. T., Stadie, N.P., Liu, X., Terreni, J., Borgschulte, A., 2021. Neutron Insights into Sorption Enhanced Methanol Catalysis. Top. Catal. 64 (9-12), 638–643. https://doi.org/10.1007/s11244-021-01461-w.
Zachopoulos, A., Heracleous, E., 2017. Overcoming the equilibrium barriers of CO2 hydrogenation to methanol via water sorption: A thermodynamic analysis. J. CO2 Util. 21, 360–367. https://doi.org/10.1016/j.jcou.2017.06.007.
Arora, A., Iyer, S.S., Hasan, M.M.F., 2018. GRAMS: A general framework describing adsorption, reaction and sorption-enhanced reaction processes. Chem. Eng. Sci. 192, 335–358. https://doi.org/10.1016/j.ces.2018.07.031.
Arora, A., Iyer, S.S., Bajaj, I., Hasan, M.M.F., 2018. Optimal Methanol Production via Sorption-Enhanced Reaction Process. Ind. Eng. Chem. Res. 57 (42), 14143–14161. https://doi.org/10.1021/acs.iecr.8b02543.
Bayat, M., Dehghani, Z., Hamidi, M., Rahimpour, M.R., 2014. Methanol synthesis via sorption-enhanced reaction process: Modeling and multi-objective optimization. J. Taiwan Inst. Chem. Eng. 45 (2), 481–494.
Bayat, M., Dehghani, Z., Rahimpour, M.R., 2014. Sorption-enhanced methanol synthesis in a dual-bed reactor: Dynamic modeling and simulation. J. Taiwan Inst. Chem. Eng. 45 (5), 2307–2318.
Bayat, M., Heravi, M., Rahimpour, M.R., 2016. Sorption enhanced process by integrated heat-exchanger reactor assisted by fluidization concept for methanol synthesis. Chem. Eng. Process. Process Intensif. 110, 30–43. https://doi.org/10.1016/j.cep.2016.09.018.
Nieminen, H., Givirovskiy, G., Laari, A., Koiranen, T., 2018. Alcohol promoted methanol synthesis enhanced by adsorption of water and dual catalysts. J. CO2 Util. 24, 180–189. https://doi.org/10.1016/j.jcou.2018.01.002.
Leperi, K.T., Yancy-Caballero, D., Snurr, R.Q., You, F., 2019. 110th Anniversary: Surrogate Models Based on Artificial Neural Networks to Simulate and Optimize Pressure Swing Adsorption Cycles for CO2 Capture. Ind. Eng. Chem. Res. 58 (39), 18241–18252. https://doi.org/10.1021/acs.iecr.9b02383.
Nieminen, H., Laari, A., Koiranen, T., 2019. CO2 hydrogenation to methanol by a liquid-phase process with alcoholic solvents: A techno-economic analysis. Processes. 7, 1–24. https://doi.org/10.3390/pr7070405.
Nyári, J., Magdeldin, M., Larmi, M., Järvinen, M., Santasalo-Aarnio, A., 2020. Techno-economic barriers of an industrial-scale methanol CCU-plant. J. CO2 Util. 39, 101166. https://doi.org/10.1016/j.jcou.2020.101166.
Boon, J., Cobden, P.D., van Dijk, H.A.J., van Sint Annaland, M., 2015. High-temperature pressure swing adsorption cycle design for sorption-enhanced water-gas shift. Chem. Eng. Sci. 122, 219–231. https://doi.org/10.1016/j.ces.2014.09.034.
Tsotsas, E., Schlünder, E.U., 1988. Some remarks on channelling and on radial dispersion in packed beds. Chem. Eng. Sci. 43, 1200–1203. https://doi.org/10.1016/0009-2509(88)85081-4.
Guffanti, S., Visconti, C.G., Groppi, G., 2021. Model analysis of the role of kinetics, adsorption capacity, and heat and mass transfer effects in sorption enhanced dimethyl ether synthesis. Ind. Eng. Chem. Res. 60 (18), 6767–6783. https://doi.org/10.1021/acs.iecr.1c00521.
Guffanti, S., Visconti, C.G., van Kampen, J., Boon, J., Groppi, G., 2021. Reactor modelling and design for sorption enhanced dimethyl ether synthesis. Chem. Eng. J. 404, 126573. https://doi.org/10.1016/j.cej.2020.126573.
Xiu, G.-H., Soares, J.L., Li, P., Rodrigues, A.E., 2002. Simulation of five-step one-bed sorption-enhanced reaction process. AIChE J. 48 (12), 2817–2832. https://doi.org/10.1002/aic.690481210.
Vande Wouwer, A., Saucez, P., Vilas, C., 2014. Simulation of ODE/PDE models with MATLAB®, OCTAVE and SCILAB. Sci. Eng. Appl. https://doi.org/10.1007/978-3-319-06790-2.
Lin, R., Liu, J., Nan, Y., DePaoli, D.W., Tavlarides, L.L., 2014. Kinetics of Water Vapor Adsorption on Single-Layer Molecular Sieve 3A: Experiments and Modeling. Ind. Eng. Chem. Res. 53 (41), 16015–16024. https://doi.org/10.1021/ie5024645.
Maksimov, P., Laari, A., Ruuskanen, V., Koiranen, T., Ahola, J., 2020. Gas phase methanol synthesis with Raman spectroscopy for gas composition monitoring. RSC Adv. 10 (40), 23690–23701.
Graaf, G.H., Sijtsema, P.J.J.M., Stamhuis, E.J., Joosten, G.E.H., 1986. Chemical equilibria in methanol synthesis. Chem. Eng. Sci. 41 (11), 2883–2890. https://doi.org/10.1016/0009-2509(86)80019-7.
Graaf, G.H., Winkelman, J.G.M., 2016. Chemical Equilibria in Methanol Synthesis Including the Water-Gas Shift Reaction: A Critical Reassessment. Ind. Eng. Chem. Res. 55 (20), 5854–5864. https://doi.org/10.1021/acs.iecr.6b00815.
Lommerts, B.J., Graaf, G.H., Beenackers, A.A.C.M., 2000. Mathematical modeling of internal mass transport limitations in methanol synthesis. Chem. Eng. Sci. 55 (23), 5589–5598. https://doi.org/10.1016/S0009-2509(00)00194-9.
B.A. Finlayson, Introduction to Chemical Engineering Computing, 2006. https://doi.org/10.1002/0471776688.
Akberov, R.R., 2011. Calculating the vapor-liquid phase equilibrium for multicomponent systems using the Soave-Redlich-Kwong equation. Theor. Found. Chem. Eng. 45 (3), 312–318. https://doi.org/10.1134/S004057951103002X.
Soave, G., 1972. Equilibrium constants from a modified Redlich-Kwong equation of state. Chem. Eng. Sci. 27 (6), 1197–1203. https://doi.org/10.1016/0009-2509(72)80096-4.
M. Sanni, Petroleum engineering: Principles, calculations and workflows, 2018. https://doi.org/10.1002/9781119387985.
Bussche, K.M.V., Froment, G.F., 1996. A steady-state kinetic model for methanol synthesis and the water gas shift reaction on a commercial Cu/ZnO/Al2O3 catalyst. J. Catal. 161 (1), 1–10. https://doi.org/10.1006/jcat.1996.0156.
Nestler, F., Schütze, A.R., Ouda, M., Hadrich, M.J., Schaadt, A., Bajohr, S., Kolb, T., 2020. Kinetic modelling of methanol synthesis over commercial catalysts: A critical assessment. Chem. Eng. J. 394, 124881. https://doi.org/10.1016/j.cej.2020.124881.
Nestler, F., Müller, V.P., Ouda, M., Hadrich, M.J., Schaadt, A., Bajohr, S., Kolb, T., 2021. A novel approach for kinetic measurements in exothermic fixed bed reactors: Advancements in non-isothermal bed conditions demonstrated for methanol synthesis, React. Chem. Eng. 6 (6), 1092–1107.
Deb, K., Pratap, A., Agarwal, S., Meyarivan, T., 2002. A fast and elitist multiobjective genetic algorithm: NSGA-II. IEEE Trans. Evol. Comput. 6, 182–197. https://doi.org/10.1109/4235.996017.
Subraveti, S.G., Pai, K.N., Rajagopalan, A.K., Wilkins, N.S., Rajendran, A., Jayaraman, A., Alptekin, G., 2019. Cycle design and optimization of pressure swing adsorption cycles for pre-combustion CO2 capture. Appl. Energy. 254, 113624. https://doi.org/10.1016/j.apenergy.2019.113624.
Hao, Z., Caspari, A., Schweidtmann, A.M., Vaupel, Y., Lapkin, A.A., Mhamdi, A., 2021. Efficient hybrid multiobjective optimization of pressure swing adsorption. Chem. Eng. J. 423, 130248. https://doi.org/10.1016/j.cej.2021.130248.
Haghpanah, R., Majumder, A., Nilam, R., Rajendran, A., Farooq, S., Karimi, I.A., Amanullah, M., 2013. Multiobjective optimization of a four-step adsorption process for postcombustion CO2 capture via finite volume simulation. Ind. Eng. Chem. Res. 52 (11), 4249–4265. https://doi.org/10.1021/ie302658y.
Wang, Z., Rangaiah, G.P., 2017. Application and Analysis of Methods for Selecting an Optimal Solution from the Pareto-Optimal Front obtained by Multiobjective Optimization. Ind. Eng. Chem. Res. 56 (2), 560–574. https://doi.org/10.1021/acs.iecr.6b03453.
R. Dorfman, Marginal Productivity Theory, in: New Palgrave Dict. Econ., Palgrave Macmillan UK, London, 2017: pp. 1–5. https://doi.org/10.1057/978-1-349-95121-5_988-2.
Catarina Faria, A., Miguel, C.V., Madeira, L.M., 2018. Thermodynamic analysis of the CO2 methanation reaction with in situ water removal for biogas upgrading. J. CO2 Util. 26, 271–280. https://doi.org/10.1016/j.jcou.2018.05.005.
An, H., Zhang, F., Guan, Z., Liu, X., Fan, F., Li, C., 2018. Investigating the Coke Formation Mechanism of H-ZSM-5 during Methanol Dehydration Using Operando UV-Raman Spectroscopy. ACS Catal. 8 (10), 9207–9215. https://doi.org/10.1021/acscatal.8b00928.
Massa, F., Coppola, A., Scala, F., 2020. A thermodynamic study of sorption-enhanced CO2 methanation at low pressure. J. CO2 Util. 35, 176–184. https://doi.org/10.1016/j.jcou.2019.09.014.
Peinado, C., Liuzzi, D., Ladera-Gallardo, R.M., Retuerto, M., Ojeda, M., Peña, M.A., Rojas, S., 2020. Effects of support and reaction pressure for the synthesis of dimethyl ether over heteropolyacid catalysts. Sci. Rep. 10, 1–12. https://doi.org/10.1038/s41598-020-65296-3.